

# Generation of spatially correlated fracture models for seismic simulations

Ravi Shekhar\* and Richard L. Gibson, Jr

Department of Geology and Geophysics, Texas A&M University, College Station, Texas, USA. E-mail: [ravisk9822213@yahoo.com](mailto:ravisk9822213@yahoo.com)

Accepted 2011 January 2. Received 2010 December 8; in original form 2010 February 7

## SUMMARY

The critical geometrical parameters that quantify the spatial distribution of natural fractures are the orientation, length and position of fractures. Knowledge of their spatial distribution is important as they control the movement of subsurface fluids and also influence seismic waves propagating in the subsurface. However, generating realistic models of all of these geometrical parameters to use in forward seismic modelling or inversion applications can become very difficult, especially when constraints are available only at a few sparse well locations. Hence, this provides strong motivation for applying seismic data to estimate these quantities in field settings, and reliable seismic modelling provides important constraints for interpretation and inversion. The Discrete Fracture Network (DFN) approach has been used frequently to generate models with stochastic distributions of fractures based on sparse well and seismic data. However, most of these studies lack any constraint from physical models of the behaviour of fractured media. In this paper, we implement and extend an alternative modelling technique to generate several realizations of a fracture model beginning with theoretical results for the strain energy of a fractured material and propose ways to better incorporate geological field observations. The method utilizes an elastic energy function that sums the interactions of all pairs of fractures present in the model. The energy for each pair depends on the distance between the two fractures, their orientations, lengths and some material properties. This energy function also serves as an objective function for a simulated annealing (SA) algorithm used to obtain multiple realizations of correlated fracture networks. We improve earlier versions of this technique by incorporating periodic boundary conditions, including criteria to limit the maximum range of pair-wise calculations and suggesting methods to constrain models to match field data. Assuming that the host rock is isotropic and homogeneous, this method produces orthogonal sets of fractures, a pattern that is commonly observed during basin formation or subsidence. This shows how the method can be utilized to provide constraints with a physical basis to facilitate the development of fracture models. We also outline how the fracture model can be converted into an anisotropic seismic velocity model to compute synthetic seismograms for reservoir characterization applications.

**Key words:** Inverse theory; Fracture and flow; Seismic anisotropy; Computational seismology; Statistical seismology; Mechanics, theory, and modelling.

## 1 INTRODUCTION

The quantification of the spatial distribution of fractures in low permeability rocks, at least for areas with both high and low fracture density zones, is essential as they control the nature of fluid flow in those rocks. To date very few studies have been performed on the spatial correlation of parameters such as length, orientation and position of fractures, though some of the studies concentrated on long-range density correlations using fractal geometry (Berkowitz

*et al.* 2000; Darcel *et al.* 2003). Bour & Davy (1999) have studied the correlation between the position and the length of the fracture. However, most of these studies either used the sparse well data or scanline data from the outcrops. Hence, utilizing seismic reflection data to determine the spatial distribution, orientations and other fracture-related properties is therefore a very important task, especially since it is otherwise difficult to obtain any information between well locations. A number of investigations have described methods for accomplishing this goal by inverting seismic data (Beretta *et al.* 2002; Angerer *et al.* 2003). However, we still lack a physically accurate method for estimating fracture distributions for both forward modelling and inversion studies. A common

\*Now at: ExxonMobil Upstream Research Company, Houston, Texas, USA.

approach used for modelling natural fractures is to apply the discrete fracture network (DFN) method, a statistical method which produces a list of locations, sizes and orientations of individual fractures. However, one of the major limitations is that the data used to populate fractures in large DFN models are either obtained from 1-D well data or scanline data that introduces significant errors into the models.

In this paper, we implement and extend a model of the spatial distribution of fractures that directly considers the elastic energy in a fractured material (Masihi & King 2007), a model that has not previously been applied in seismic applications. The modelling is based on the assumption that the elastic free energy associated with the fracture distribution follows the Boltzmann distribution. The expression that determines the spatial correlation function for the displacement of fractures is used as an objective function to generate several realizations for fracture distributions using a simulated annealing (SA) algorithm that minimizes that objective function. The basic assumption for this method is that the reference rock sample used for study is already fractured and the rock sample has already achieved mechanical equilibrium. This equilibrium assumption allows us to use entropy arguments and statistical mechanics for modelling fractures. The first general goal of the paper is therefore to review and to extend this stochastic modelling technique to develop a method for simulating fracture distributions in large, field-scale settings for seismic and flow studies. We then show how to incorporate periodic boundary conditions (PBC) into the simulations, describe criteria to limit the maximum range of pair-wise interactions, and suggest methods to constrain models to match field data. Finally, we show how the stochastic models generated with this concept can be converted into anisotropic seismic velocity models to simulate 3-D seismic surveys.

## 2 ELASTIC ENERGY FUNCTION FOR SPATIALLY CORRELATED FRACTURES

This section discusses the important steps involved in the derivation of the energy function for the spatial correlation of the elastic displacement of fractures, which also serves as the objective function for the SA algorithm. The complete derivation is given in Shekhar (2008). We write the vector displacement field within the fractured rock volume as  $\mathbf{u}(\mathbf{x}) = \mathbf{x} - \mathbf{x}'$ , noting that the particle at  $\mathbf{x}$  has moved to  $\mathbf{x}'$ . Beginning with the theoretical expressions suggested by Landau & Lifshitz (1982b, chapter IV) that describe elastic deformations in the presence of dislocations, Masihi & King (2007) propose a model in which a fracture is defined as a discontinuity in the displacement vector. Therefore, the displacement vector is assumed to have continuous part (elastic displacement  $\mathbf{u}^e$ ) and a discontinuous part (the inelastic displacement  $\mathbf{u}^i$ ). The latter acts as a source term for inelastic strain. Similarly, the strain and stress can be decomposed into elastic and inelastic parts,

$$e_{ij} = e_{ij}^e + E_{ij} \quad \text{and} \quad \sigma_{ij} = \sigma_{ij}^e + S_{ij}. \quad (1)$$

If the system is in mechanical equilibrium, that is, in the absence of any external body forces, the equation of continuity becomes,

$$\partial_j \sigma_{ij} = \partial_j \sigma_{ij}^e + \partial_j S_{ij} = 0 \quad \text{or} \quad \partial_j \sigma_{ij}^e = -\partial_j S_{ij}, \quad (2)$$

where the inelastic part of stress, the internal sources of stress, becomes the fictitious body force that gives rise to displacement and fracturing and also keeps fractures open. Heffer & King (2006) note that the total elastic energy per unit volume required to keep fractures open is the work done by elastic forces on the total strain.

This total elastic energy is given as

$$E = \frac{1}{2} \sigma_{ij}^e \epsilon_{ji}^e. \quad (3)$$

Assuming isotropic stress conditions and using Fourier transforms of stress and strain fields and contracting terms as in eq. (3), the expression for the elastic energy is

$$\begin{aligned} E(\mathbf{k}) &= \frac{1}{2} [(\lambda + \mu)k_k k_l + \mu k^2 \delta_{kl}] u_k^e(\mathbf{k}) u_l^e(-\mathbf{k}) \\ &= \frac{\mu}{2} L_{kl}(\mathbf{k}) u_k^e(\mathbf{k}) u_l^e(-\mathbf{k}), \end{aligned} \quad (4)$$

where  $L_{kl}$  is the linear operator of isotropic elasticity and is the inverse of the Green's function,  $L_{kl} G_{lm} = \delta_{km}$ . Applying the assumption that the frequency distribution,  $p(E)$ , of strain energy due to the displacements/dislocations or fractures follows the Boltzmann Law,

$$p(E) \propto \exp(-E / \langle E \rangle), \quad (5)$$

implies that the dislocations or fractures adopt a configuration that maximizes the entropy of the system subject to mean strain energy,  $\langle E \rangle$ , being fixed. This assumption leads to the following expression for the spatial correlation between the elastic displacements or fractures in real space,

$$\begin{aligned} C_{kl}(\mathbf{r}) &= \frac{\langle E \rangle}{\mu} \bar{G}_{kl}(\mathbf{r}) \\ &= \frac{\langle E \rangle}{16\pi\mu(1-\nu)} \left( \frac{(3-4\nu)\delta_{kl}}{r} + \frac{\mathbf{r}_k \mathbf{r}_l}{r^3} \right), \end{aligned} \quad (6)$$

where the terms  $\mu$ ,  $\nu$  are the shear modulus of elasticity and the Poisson ratio of the rock sample, respectively. Realizations of the random fields described by this covariance relationship will satisfy eq. (2), which can be used to determine both  $\sigma_{ij}^e$  and  $\epsilon_{ji}^e$ . Using general results for spatial correlations of vector fields (Daly 2001), it can be shown that the energy function for the above distributions of fractures can be written as (Shekhar 2008)

$$\begin{aligned} E &= \sum_{k=1}^N \sum_{\substack{l=1 \\ k \neq l}}^N A u_k u_l [\eta |\cos(\theta_k - \theta_l)| \\ &\quad + |\cos(\alpha - \theta_l) \cos(\alpha - \theta_k)|] / r_{kl}, \end{aligned} \quad (7)$$

where  $A = \langle E \rangle / 16\pi\mu(1-\nu)$ ,  $N$  is the number of fractures in the system, and the components  $u_k$  and  $u_l$  are the displacements on fractures in  $k$  and  $l$  direction.  $\alpha$ ,  $\theta_k$  and  $\theta_l$  specify the orientations of the distance vector  $r$  and fracture vectors  $u_k$  and  $u_l$  with respect to the horizontal  $x$ -axis. This equation relates the pairwise interactions of fractures to the total elastic energy of the system.

## 3 METHOD FOR MODELLING FRACTURE DISTRIBUTIONS

A set of fractures that minimizes the energy function in eq. (7) will satisfy the physical model used in its derivation, which assumes equilibrium. This requires the choice of an optimization algorithm that allows a minimum to be found for arbitrary fractures. SA is in fact such a stochastic optimization method that has been used in variety of problems that involve finding global optimum values of a function consisting of large number of independent variables (e.g. Tran 2007). Below we outline our implementation of SA for the estimation of fracture distributions. We then describe our choice of PBC, including parameter choices for minimizing computation time. This section concludes with test applications illustrating the

sensitivity of the algorithm to important model parameters and suggests several steps to constrain results to fit field observations such as fracture orientations detected from core, image logs or seismic attributes.

### 3.1 SA algorithm

To apply the SA optimization algorithm for any problem, one must define several important quantities: initial description of sets of possible configurations of the system, probability distributions used for updating unknown parameters, an energy function  $E$  (analogue of energy) used for global minimization, a control parameter  $T$  (analogue of energy) and an annealing schedule of changing a temperature-like parameter, so that system can reach its equilibrium.

In the application of SA to the current fracture modelling problem, the objective function is the elastic energy function (eq. 7), while the fracture model parameters such as position, length and orientation are the quantities that are selected for an optimal, low-energy configuration. The first step in the application of SA is to choose the initial fracture configuration. Because most model perturbations are accepted during the initial stages of the SA procedure, the model can become quite different from the initial configuration, and the choice of the initial model is not too important. For this reason, we can start with any configuration of fractures having length  $l$  and orientation  $\theta$  in a square system of side length  $L$ . We start with the calculation of initial energy of the fracture configuration,  $E_i$ , using eq. (7). The initial temperature,  $T_i$ , is chosen of the same order of magnitude as the initial energy value so that the acceptance ratio at the start is approximately 99–100 per cent. To change the current configuration of fractures, a fracture  $j$  is selected randomly and its length, orientation and/or position are changed slightly. The distribution functions used for selecting updates to the orientation, length and the position are identical to Masihi & King (2007)

$$\theta_j^{\text{new}} = \theta_j + 0.05\pi(2R - 1) \quad (8a)$$

$$l_j^{\text{new}} = l_j + 0.5(2R - 1) \quad (8b)$$

$$r_j^{\text{new}} = r_j + 0.5(2R - 1), \quad (8c)$$

where  $R$  is a random number selected from a uniform distribution in the range of  $[0-1]$ . Once again the energy of the new state of the configuration,  $E_{i+1}$ , is calculated using eq. (7). To determine the acceptance of the new, perturbed configuration,  $E_{i+1}$ , with respect to previous configuration,  $E_i$ , the change in energy  $\Delta E = E_j - E_i$  is calculated assuming  $A$  to be one as it is just a scaling factor. If  $\Delta E < 0$ , then perturbed configuration is accepted unconditionally and we go back to previous step with  $E_i = E_{i+1}$ . If  $\Delta E > 0$ , then the new perturbed state is accepted or rejected on the basis of the Metropolis algorithm. This means that a new state escapes from local minima. This step is performed for 20–30 iterations at a particular temperature where every fracture is visited at every iteration. Then the temperature parameter is changed using the exponential cooling schedule  $T^{\text{new}} = \alpha T^{\text{old}}$  where  $\alpha = 0.97$ . Here, we take a large number of temperature iterations, assuming the function reaches an optimal minimum of the solution after a significantly large number of iterations.

### 3.2 PBC implementation

To apply the SA algorithm, we choose a model of finite size having a finite set of fractures. Since the model that we have chosen has a limited lateral dimension, the associated truncation at the boundaries of the model can introduce artificial effects in the final configuration of fractures from SA. So, an accurate understanding of the effects of boundaries on the overall fracture configuration becomes very important. This is because fractures close to the boundary experience different effective stress, hence energy, compared to fractures in the centre of the model. Also, while changing the configuration of fractures by perturbing their position some fractures close to the boundary can move out of the model, thus affecting the number density of fractures. These limitations can affect our model of the final configuration of the fracture system. So, to eliminate these problems, PBC are applied to the original model area. In principle, this would lead to an infinite number of pairs of fractures during the application of SA using the sum in eq. (7). One of the major concerns while applying the PBC is how to truncate calculations without losing accuracy. Masihi & King (2007) also apply a PBC, and, although they state that they used two repeated model areas, they do not present results to explain their choice of parameters. For the sake of completeness, we will show selected results to show how to implement the PBC and to support our truncation parameters selection. Specifically, we can establish criteria for determining the maximum distance, and number of repeated model cells, which must be considered in implementing the PBC in the SA code using a simple test model. This model includes 2500 fractures in a square area 5000 m on each side, each fracture 50 m in length with a random orientation between  $-30^\circ$  and  $+30^\circ$  (Fig. 1). This model was used to estimate the maximum distance at which significant fracture interaction occurs. In other words, we needed to determine the distance up to which a slight change in fracture configurations influence other fractures or affects the total energy value. The most important factors are relative orientation of fractures and ratio of length of fractures. For detailed analysis, an arbitrary fracture (the first fracture of the test model) was taken and the total initial energy was calculated using eq. (9).

$$E_i = \sum_{\substack{l>1 \\ k=1}}^N Au_k u_l [\eta |\cos(\theta_k - \theta_l)| + |\cos(\alpha - \theta_l)\cos(\alpha - \theta_k)|] / r_{kl}. \quad (9)$$

The effect of the orientation of other fractures was then quantified by recomputing the total energy value while rotating a single fracture at  $r = (100,50), (200,50), (300,50), \dots, (4000,50)$ , etc. one at a time, changing the orientation by  $15^\circ$  (Fig. 2a). The influence of fracture length as a function of the separation between fractures was tested in the same way (Fig. 2b). The results confirm that fractures close to the reference fracture have significantly larger influence than fractures at a distance, which is not surprising given that energy is inversely proportional to distance (eq. 9). In fact, fractures at distances larger than  $r = 1200$  m have negligible influence on total energy value. So, for our modelling study the cut-off radius ( $r_{\text{cut-off}}$ ), the distance up to fractures influence each other, is 1200 m. Hence, the minimum number of periodic images required for an accurate PBC can be calculated as follows: if  $r_{\text{cut-off}} > a$  then  $N = r_{\text{cut-off}}/a$ , else  $N = (r_{\text{cut-off}}/a) + 1$ . Here  $a$  is the one side of square representative model and  $N$ , the largest integer value, is the number of model images required for the PBC. So the number of periodic images surrounding the model cell will be equal to  $N$  in both side in  $x$ - and  $y$ -directions to neutralize the effect of boundaries of the model cell. The PBC can be implemented by copying enough images of the model to extend

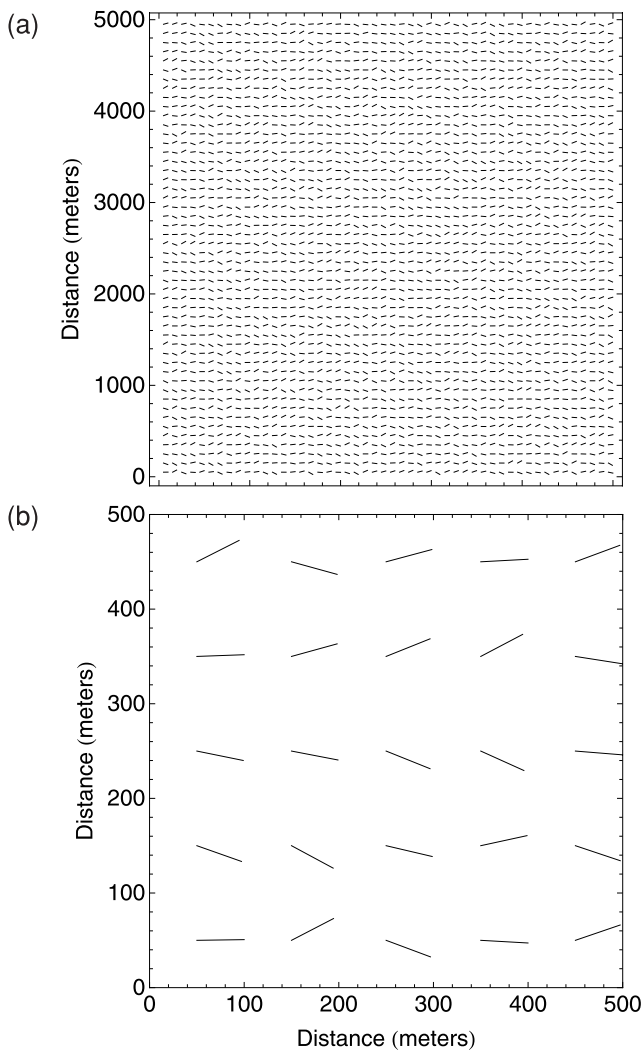


**Figure 1.** The starting model used for testing the parameters affecting periodic boundary condition implementations. This model consists of 2500 fractures in a square area with each side 5000 m. (a) Complete fracture distribution. (b) Detail view of fracture distribution.

to a distance of  $r_{\text{cut-off}}$  in all directions. Shekhar (2008) presents examples of model distortions arising when inadequate PBCs are applied.

### 3.3 Parameter sensitivity and model constraints

The goal of this section to present examples of the modelling scheme, to understand the sensitivity of results to model parameters, and suggest methods for constraining models to field observations. The most important model parameters in the objective energy function used for SA algorithm are length, orientation and position of fractures. Any slight change in any of these parameters affects the final configuration of fractures and the decrease in the energy function. Here, we show these effects by slightly changing either one parameter or a combination of parameters in the SA algorithm. We will also examine non-uniqueness in models. We started with an initial model containing 100 fractures with lengths selected from a Gaussian distribution (mean 50 m,  $SD$  20 m) to study sensitivity (Fig. 3a). The model parameters were then perturbed using eq. (8). Fig. 3(b) shows the effect of perturbation of orientation only and of simultaneous perturbation of orientation and length on the energy

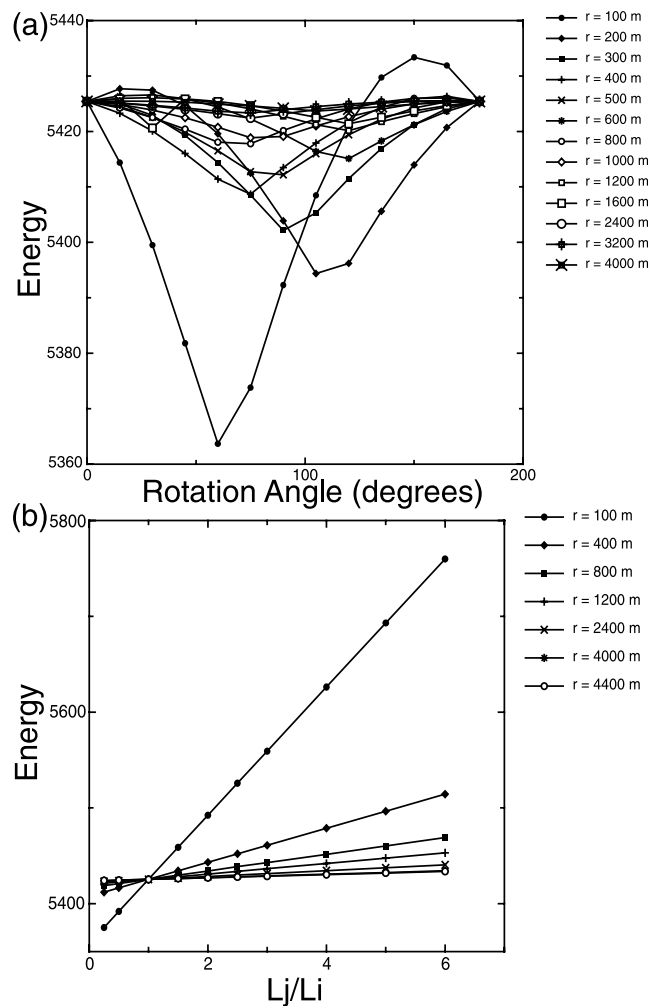


**Figure 2.** (a) The effect of rotation (relative orientation) of a fracture on total energy value. Here  $r$  is the  $x$  coordinate of the test fracture that is rotated; the  $y$  coordinate of the test fracture was 50 m. (b) The effect of relative fracture lengths on total energy value. Here,  $L_i$  is the first fracture and  $L_j$  is the fracture whose length is changed. See text for details of the test procedure.

function. As is typical in SA applications, the energy function fluctuates significantly for the first few iterations at high  $T$ , because a large number of perturbations/realizations are accepted, but fluctuations decrease at later iterations when many fracture configurations are rejected. The energy function becomes stable at around 6000 iterations, suggesting that the energy function is close to minimum (Fig. 3b).

Another aspect of the parameter perturbation procedure (eq. 8b) is that successive iterations can eventually make a fracture length negative, which is not possible. The energy function can also be minimized by reducing lengths to zero, which is an uninteresting, trivial solution. It is therefore important to renormalize fracture lengths at the end of each iteration so that the mean length of fractures remains the same as values observed in any available field data or the initial mean length of the starting model. Fig. 3(b) compares the change in the energy function with the number of iterations for cases with and without this renormalization to mean length. Both cases apply an additional constraint forcing lengths to fall between specified minimum and maximum values (30 m and 70 m in this case). The figure clearly shows that if the fracture length is renormalized to the mean

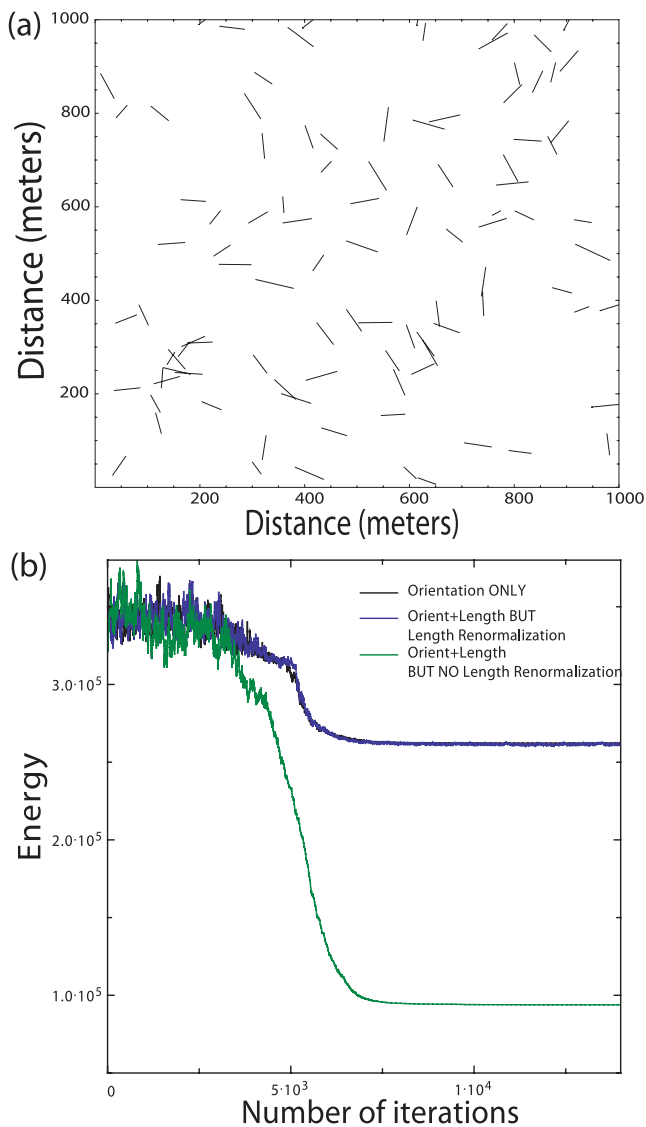


**Figure 3.** (a) Original model of 100 fractures with Gaussian distribution of length of mean = 50 m and  $SD = 20$  m (b) Comparison of energy value for different cases after 14 000 iterations. Note that when fracture length is renormalized, the energy level is essentially the same as for changes in orientation only and the two curves are hard to distinguish.

value, the energy function coincides with the case of orientation perturbation only (Fig. 3b). This is because the energy can be greatly reduced by minimizing fracture lengths, whereas constraining the mean value to be unchanged keeps a higher energy level. Fig. 3(b) also shows that for the case of orientation and length perturbation without renormalization, the energy function continues decreasing until all fractures reach the minimum length constraint. Hence, this test shows that the length of fractures needs to be first constrained to minimum and maximum values and then renormalized to the mean length of fractures. Fig. 4 shows the final orientation and length distribution of fractures for all three cases. For the case when the length is renormalized, the energy function reaches a minimum with a bimodal distribution of fracture lengths and orientations, whereas for the case without renormalization, the energy is minimized when fracture lengths are unimodal (minimum length). Note that for the case of orientation updates only, the distribution of lengths reflects the Gaussian distribution used to select the initial model configu-

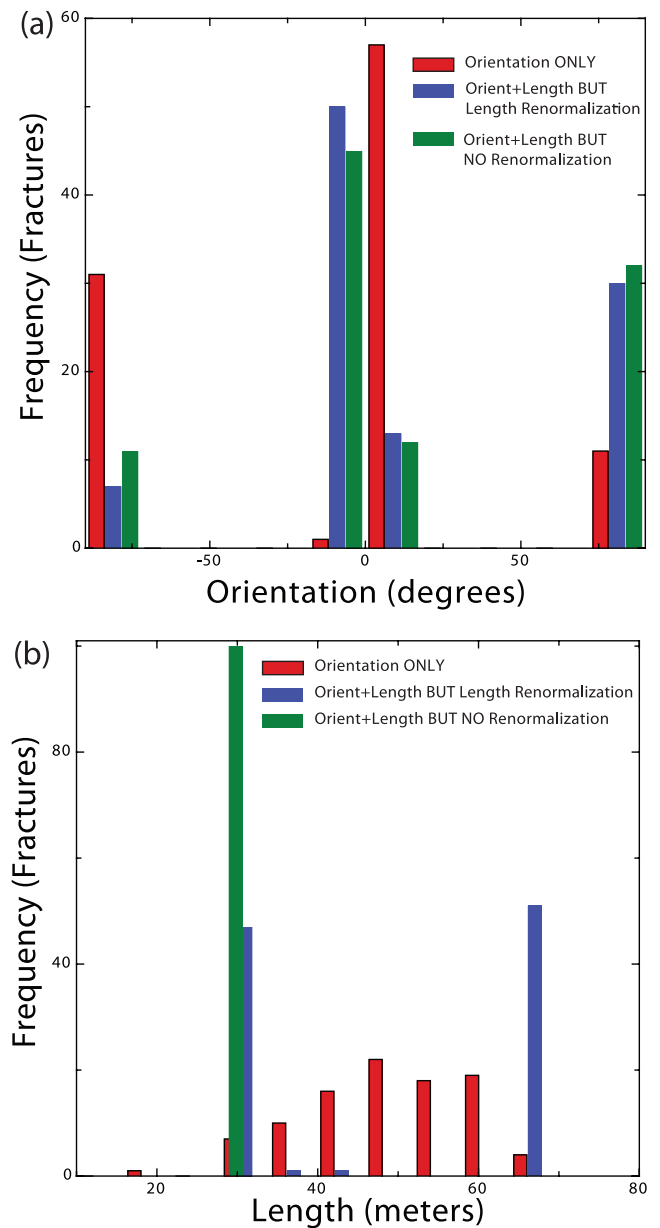


**Figure 4.** Distributions of orientation and lengths of fractures after application of simulated annealing algorithm to model in Fig. 3a. (a) Final orientation of fractures. (b) Final length of fractures.

ration. In this demonstration, the constraints on fracture length are very simple, but more complete applications could apply similar constraints to more complex distributions. Note also that there are two general sets of fractures separated by  $90^\circ$  in orientation. The orthogonal pattern of fractures generated from this model is commonly observed during basin formation or subsidence (Belayneh *et al.* 2007). More detailed analysis suggests surprisingly that the fractures orientations can still change, though they remain orthogonal. This is because the energy function (eq. 7) depends only on the relative orientation of fracture pairs. The total system of fractures can be rotated arbitrarily without changing the energy value.

A similar study was performed by perturbing the position of fractures using the same initial model, using eq. (8c), to study how fracture location influences the energy function. This will provide insights into the maximum change in location of individual fractures. This information is important as it can help in assigning the

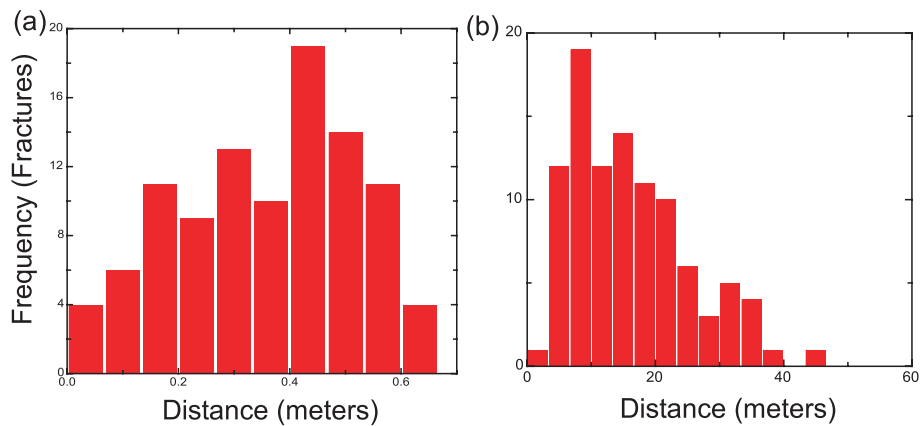


**Figure 5.** Histograms showing (a) total fracture displacement (distance from initial position) after the first simulated annealing iteration, and (b) total fracture displacement after 2000 iterations.

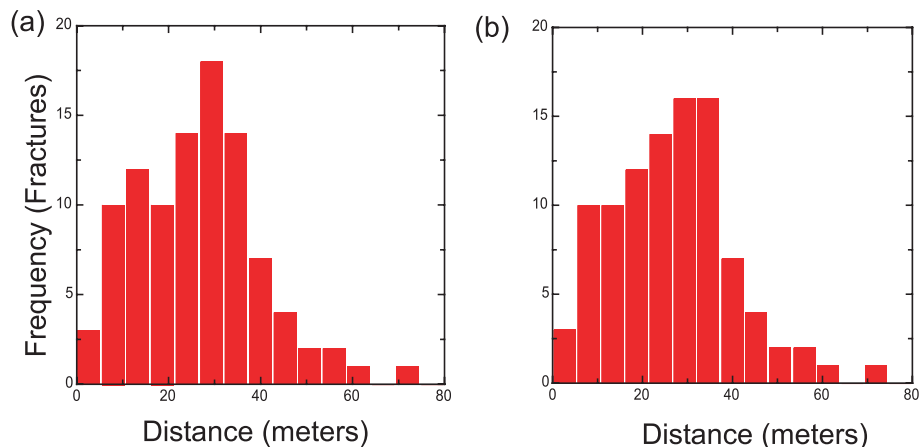


**Figure 6.** Histograms showing that (a) total fracture displacement (distance from initial position) after 8000 iterations is less than 75 m, and that (b) total fracture displacement after 10 000 iterations is still less than 75 m.

most probable initial position of each fracture in the starting model. In cases where background geological knowledge includes some estimates of lateral variations in fracture intensity, it will be easier to define useful initial spatial distributions of fractures. In this test, we calculated the total movement of fractures at each iteration by summing the distances corresponding to the change in locations of each individual fracture relative to the location at the previous iteration. The histogram of total fractures motion at several steps in the SA minimization is shown in Figs 5 and 6. The histograms suggest that the total motion of fractures is large at higher temperature, ranging from 0.5 m to about 40 m for the first 2000 iterations. However, as the temperature decreases, the increase in total movement also decreases, ranging from approximately 0 m to 60 m around 4000 and 6000 iterations. As the system moves to equilibrium and temperature decreases, there is less change in fracture position, as we see that from iteration 8000 to 10 000, the positions are almost unchanged. In general, the total displacement is constrained to fall in the range 0–75 m as shown in Fig. 6, which is less than a simulation cell size.

#### 4 INCORPORATING FRACTURE MODELS IN SEISMIC APPLICATIONS

The method of generating physically meaningful fracture distributions discussed in the previous section can be implemented for any

realistic geological field, assuming the rock to be homogenous and isotropic. Such a fracture model can in turn be utilized for various applications, and Masihi & King (2007) considered an application to fluid flow. In this section, we will instead show the application of this modelling technique to seismic modelling at field scale. To do so, we will consider a hypothetical field example that has a fixed number of fractures. We will apply arbitrary values for the mean fracture lengths, the regional trend of fracture orientation, and other spatial distribution parameters. Future applications to specific sites could easily obtain the relevant values using, for example, outcrop studies, core samples, image logs, structural geology analyses and seismic attributes. These are the same forms of data utilized in conventional DFN schemes and applying such constraints is no more difficult for the current approach (Angerer *et al.* 2003). The test example will illustrate how the parameters can be used to constrain a simulated fracture model generated from the SA algorithm to match observations from a particular field.

#### 4.1 Model description

The starting model is 920 m  $\times$  920 m, containing 3000 fractures. The initial distribution of fractures had random orientation, showing a preferential spatial trend along the diagonal as shown in Fig. 7(a). We then applied the SA method, visiting each fracture 30 times at a particular  $T$  value. At each iteration, orientation, length and

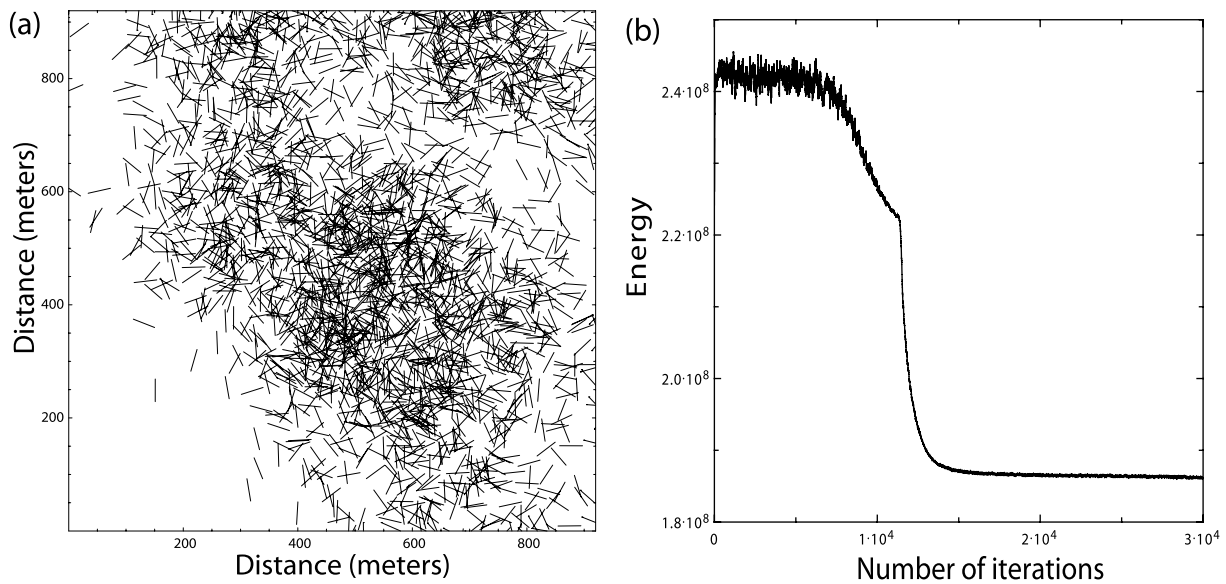


**Figure 7.** (a) Starting model of 3000 fractures having random orientation, trending along NW–SE direction. (b) Energy versus number of iteration for simulating 3000 fractures using energy method.

position of each fracture was changed using the same perturbation algorithm as discussed previously (eq. 8). Here also we rescaled the length of fractures at each iteration such that the mean length (40 m) of the fracture system remains constant. Fig. 8(b) shows the final orthogonal fracture model after 30 000 iterations (1000 reductions in temperature  $T$  and 30 visits to each fracture at every temperature). Fig. 7(b) shows the corresponding plot of energy versus iteration number. As expected, the energy function shows a large number of acceptances at the beginning (high temperature), and becomes stable as the number of iterations increases (low temperature), thus increasing the number of rejections. Recalling that minimization constrains only relative orientation of fractures, we can rotate the entire model arbitrarily as desired. In this hypothetical case, if we assume a desired regional orientation of fractures of either  $45^\circ$  or

$135^\circ$ , we can rotate the final fracture model by  $45^\circ$  to achieve the desired configuration (shown in Fig. 8).

#### 4.2 Seismic velocity model

Our goal is to utilize the fracture distribution in Fig. 8 for applications such as hydrocarbon reservoir characterization, assuming that the axes in illustration represent the two horizontal coordinates  $x$  and  $y$ . For meaningful applications, the reservoir will also have a thickness in the third coordinate direction, depth. We will therefore assume that the fractures extend from top to bottom of the layer and that the figure represents a cross-section at an arbitrary depth within that layer. The SA procedure determining the locations and

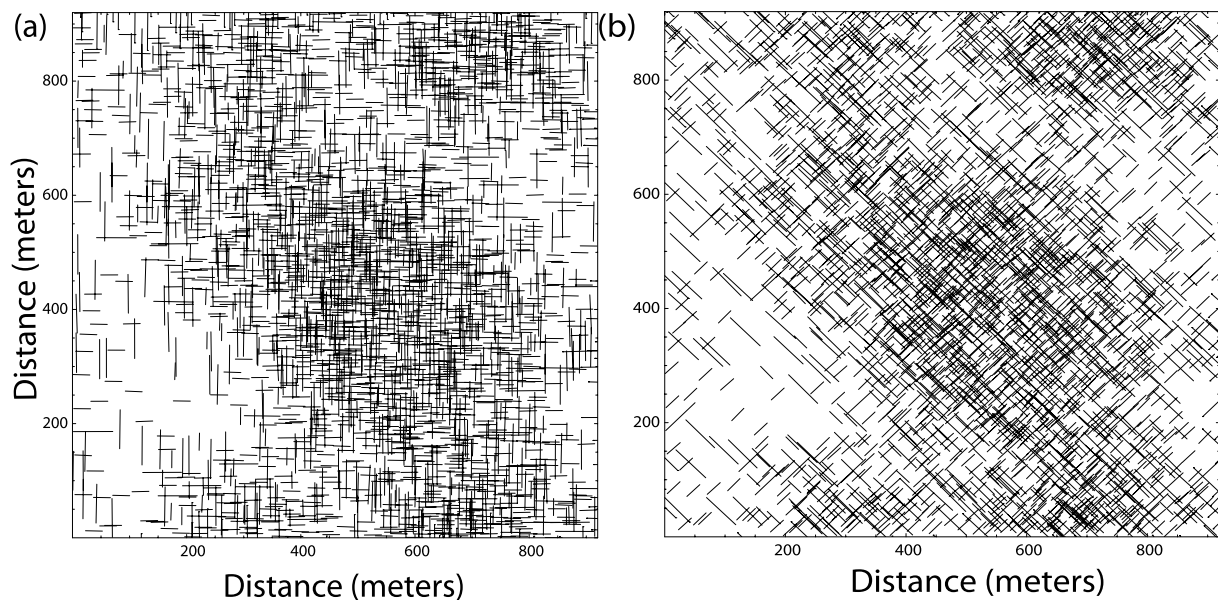


**Figure 8.** Simulated annealing results for the test model shown in Fig. 7. (a) Result generated directly by the simulated annealing. (b) Results rotated  $45^\circ$  to match hypothetical field observations.

orientations of the fractures thus ignores this thickness, which in principle could be taken into account with a significant increase in computational time (Masihi *et al.* 2007). However, as long as the reservoir thickness is relatively small compared to the lateral distances in the model, variations in depth will not have a major affect on the energy in eq. (7) and can be ignored. We will therefore assume that the reservoir layer thickness is relatively small in designing our test model below, with a value of 10 m.

The next task in relating a discrete fracture representation such as the result in Fig. 8 is to identify the theoretical basis for estimated the change in elastic moduli caused by the presence of fractures. Many solutions have been investigated over the last several decades, with various levels of accuracy and complexity (Kachanov 1980; Hudson 1981; Kachanov *et al.* 1994; Sayers & Kachanov 1995; Liu *et al.* 2000; Pointer *et al.* 2000; Tod 2001; Chapman 2003; Maultzsch *et al.* 2003; Agersborg *et al.* 2007). Furthermore, in more recent years, numerical methods have been applied to better determine the accuracy of many of the analytic solutions for the material properties of media with fractures, studying the influence of crack density and the interactions of cracks in more intensely fractured materials (Coates & Schoenberg 1995; Saenger & Shapiro 2002; Vlastos *et al.* 2003, 2007; Grechka 2005; Grechka & Kachanov 2006b). Here our primary goal is to illustrate a general approach for relating the fracture model to seismic properties, and there are several important issues. First, we note that the final fracture distribution contains two orthogonal fracture sets, which will in turn correspond to an anisotropic elastic medium (Bakulin *et al.* 2002; Grechka & Kachanov 2006b). A convenient approach for modelling the properties of these materials is that presented by Kachanov (1980) and developed by numerous workers in recent years (Sayers & Kachanov 1991; Sayers 2002; Schubnel & Guéguen 2003; Grechka & Kachanov 2006b; Hall *et al.* 2008; Guéguen & Sarout 2009). This approach relates changes in the compliances of the elastic medium to the orientations and densities of one or more fractures sets in the material. Although fluids can have important and interesting affects of propagating seismic waves (Pointer *et al.* 2000; Chapman 2003; Vlastos *et al.* 2006), we will assume they are dry in our results below for the sake of simplicity. A convenient presentation of the relevant expressions for the effective properties of the fractured medium is given in Grechka & Kachanov (2006b), who note that that material is almost always nearly orthorhombic, with four unique elastic moduli when the fractures are empty. Similar model configurations were examined by Saenger & Shapiro (2002).

Writing the general form for the effective compliances  $s_{ijkl}^e$  of the fractured rock material as the sum of the background compliance  $s_{ijkl}^0$  and perturbations  $\Delta s_{ijkl}$ ,

$$s_{ijkl}^e = s_{ijkl}^0 + \Delta s_{ijkl}, \quad (10)$$

for the dry fracture case, the perturbation terms for  $L$  sets of fractures become (Grechka & Kachanov 2006b)

$$\begin{aligned} \Delta s_{ijkl} &= \frac{8(1-\nu^2)}{3E(2-\nu)} (\alpha_{il}\delta_{jm} + \alpha_{im}\delta_{jl} + \alpha_{jl}\delta_{im} + \alpha_{jm}\delta_{il} + 4\beta_{ijlm}) \\ \alpha_{ij} &= \sum_{l=1}^L \epsilon_l n_i n_j \\ \beta_{ijkl} &= -\frac{\nu}{2} \sum_{l=1}^L e_l n_i n_j n_k n_l. \end{aligned} \quad (11)$$

Here  $\nu$  is the Poisson ratio of the host rock,  $\delta_{ij}$  is the Kronecker delta symbol,  $E$  is Young's modulus and  $\epsilon_l$  is the crack density of

crack set  $l$ . When  $a$  is the radius of these cracks, it is  $\epsilon_l = N_l a^3 / V$ , where  $V$  is the volume of the material and  $N_l$  is the number of cracks of that orientation and radius (we assume constant radius for the fractures). Given these compliances, the corresponding elastic moduli  $c_{ijkl}$  are straightforwardly computed and used in simulation of seismic wave propagation.

A key step for utilizing the fractures models provided by the SA is to calculate the crack density  $\epsilon$ , a value determined for penny-shaped cracks in the results outlined above. However, the fractures from the SA model are rectangular, with lengths determined in the SA minimization procedure and a height assumed equal to the layer thickness, 10 m. For this reason, we follow the conceptual approach of Liu *et al.* (2000) and also replace the large, rectangular fracture with a set of smaller, circular fractures of equal total area for the purposes of estimating elastic properties of the formation. The effects of the circular cracks are assumed to be essentially the same as the original fracture model. To carry out this process, we discretized the model into square cells 44 m on a side. We then computed the effective crack radius for each grid, assuming that total area occupied by rectangular fracture in each grid remains same if they are replaced by same number of circular cracks. This can be expressed as

$$\sum_{i=1}^{n_j} A_{\text{rectangular},j} = \pi a^2 N_j, \quad (12)$$

where  $n_j$  is the total number of rectangular fractures in the cell,  $a$  is the radius for each crack, which we take to be 0.5 m for the example here and  $n_j$  is the total number of circular cracks in  $j$ th cell. So, the crack density in the  $j$ th cell is  $\epsilon_j = n_j a^3 / V$  where  $v_j = N_j / V$  and  $V$  is volume of the cell. This calculation of crack density was carried out for each of the two sets of fractures (Fig. 9). In our results, the final fracture distributions consist of two sets of fractures that are orthogonal, and in any one location, the densities are very similar (8). Waves travelling in the directions of the two horizontal symmetry axes will have the similar velocities since they will be propagating parallel to one fracture set and perpendicular to the other, so that the material will be close to one that is transversely isotropic with a vertical axis of symmetry. All modelling correctly simulates reflections from the orthorhombic medium, however.

There are potential difficulties that may arise in the application of this approach. First, it is possible for large crack density values to result. Theories that do not explicitly take interaction of individual cracks or fractures into account may therefore have errors when density increases, leading to poor estimates of effective properties (Saenger & Shapiro 2002). On other hand, it is likely that in many cases analytic and numerical results suggest that the interaction effects can cancel out, minimizing errors (Kachanov 1992, 1993; Grechka & Kachanov 2006a). In our case, we also note that the estimated crack densities depend on the chosen value of crack radius  $a$ , so that the fitting predicted seismic response to field data would require an estimate of this parameter as well. This is a consequence of the conceptual step of relating the rectangular fractures to seismic properties; selecting an appropriately small value of  $a$  will lead to crack densities small enough to calculate reasonable results. Similarly, though fracture maps such as that shown in Fig. 8 may appear to exceed the critical threshold beyond which no solid continuum exists, when considering each fracture as a set of circular cracks, the solid regions surrounding each individual flaw can still maintain continuity. This becomes more evident when choosing smaller radii that lead to smaller crack densities.



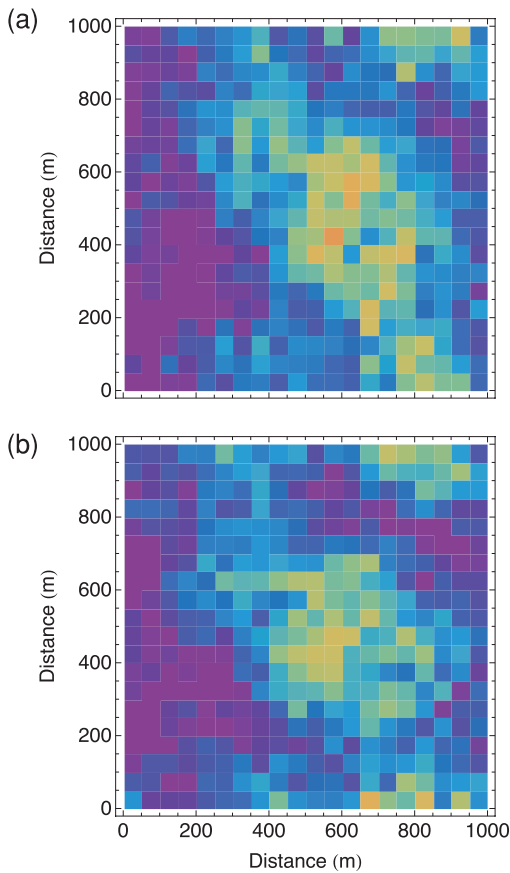


**Figure 9.** Maps of crack densities computed using eq. (12) for each set of fractures in Fig. 8. (a) map for orientation  $45^\circ$ ; (b) map for fractures with  $135^\circ$  orientation.

The calculation of the effective properties also requires values for the properties of the unfractured host rock. These values, along with those for the layers above and below the fractured layer are given in Table 1.

Approximate perturbation methods are convenient for computing synthetic seismograms in this case, where the reservoir model is strongly 3-D and anisotropic. We therefore utilize a ray-Born algorithm (Beydoun & Mendes 1989; Gibson *et al.* 1993). This method applies the Born approximation to calculate the amplitudes waves scattered by localized features in a smoothly varying background medium. In the Born approximation, all wave propagation is modelled as taking place within that background, and it is therefore convenient and accurate to use fast ray methods for computing Green's tensors. More details on the implementation and applications of such methods can be found in several sources (Beydoun & Mendes 1989; Gibson *et al.* 1993; Gibson & Thore 2009). In our study, velocities and density of overburden layers are assumed to be homogenous. Though the solution neglects traveltimes variations as-

**Table 1.**  $P$ -wave velocity  $\alpha$ ,  $S$ -wave velocity  $\beta$  and density  $\rho$  used for the seismic modelling. The host rock is the material containing the fractures, and the isotropic material above and below the reservoir has the properties of the background medium.

Property	Host rock	Background
$\alpha$	$4.25 \text{ km s}^{-1}$	$4 \text{ km s}^{-1}$
$\beta$	$2.35 \text{ km s}^{-1}$	$2.2 \text{ km s}^{-1}$
$\rho$	$2.2 \text{ g cm}^{-3}$	$2.2 \text{ g cm}^{-3}$

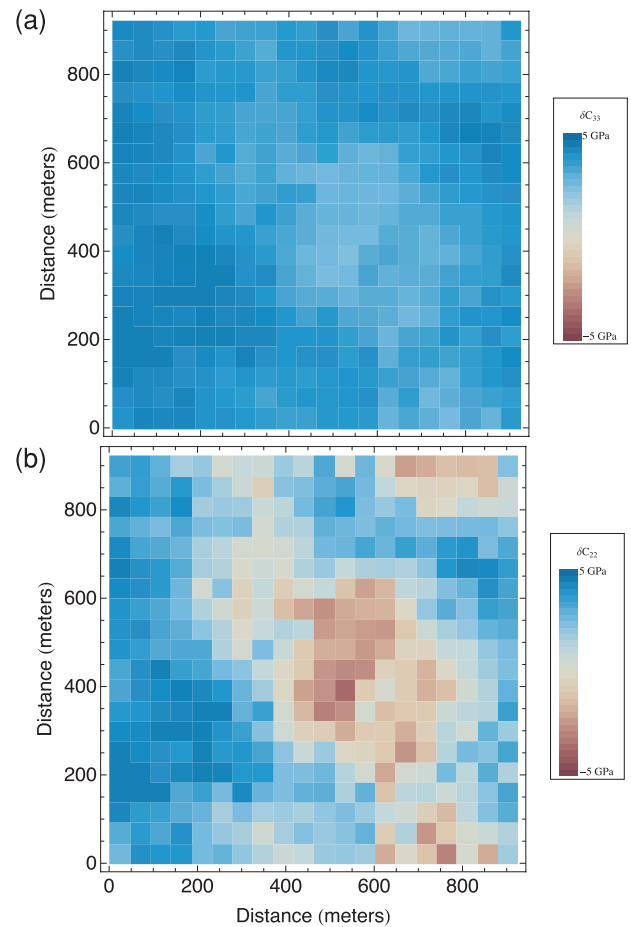


**Figure 10.** Perturbations to (a) the elastic moduli  $C_{33}$  and (b)  $C_{22}$  for the fracture model in Fig. 8.

sociated with velocity variations, it will still be accurate in this case where the fractured reservoir model layer is thin and such effects are negligible.

For simplicity, we simply parameterize the model such that the 10 m thick fractured layer is represented in terms of perturbations obtained by subtracting properties of the background medium (Table 1) from those of the fractured layer that are computed using the effective medium theory. Since the modelling results will show amplitudes of reflected  $P$ -waves, we show here perturbations to moduli  $C_{22}$  and  $C_{33}$  in the model (Fig. 10). Since the fractures are vertical, the variations in  $C_{33}$  are relatively small, though the values still increase in the regions with highest concentrations of fractures. On the other hand, the perturbation to  $C_{22}$ , which is the same as the perturbation to  $C_{11}$ , is large. Note that if no fractures were present, the perturbation in both parameters would be a constant value of 8 GPa. The fractures reduce the contrast in  $C_{33}$ , implying a weaker, but still positive, change in that parameter from the background medium to the fractured layer. However, the perturbation for  $C_{22}$  becomes negative, implying that horizontal  $P$ -wave velocity is less than in the background medium.

We computed three sets of synthetic seismograms using the ray-Born algorithm to illustrate the general behaviour of the model, where the top of the orthorhombic, fractured layer was assigned to a depth of 1000 m. In each case, there was a 37 by 37 horizontal grid of source/receiver pairs with midpoints covering the entire range of the model (25 m spacing in both  $x$  and  $y$  directions). The offset between source and receiver was set to 0 m, 728 m and 1456 m for the three

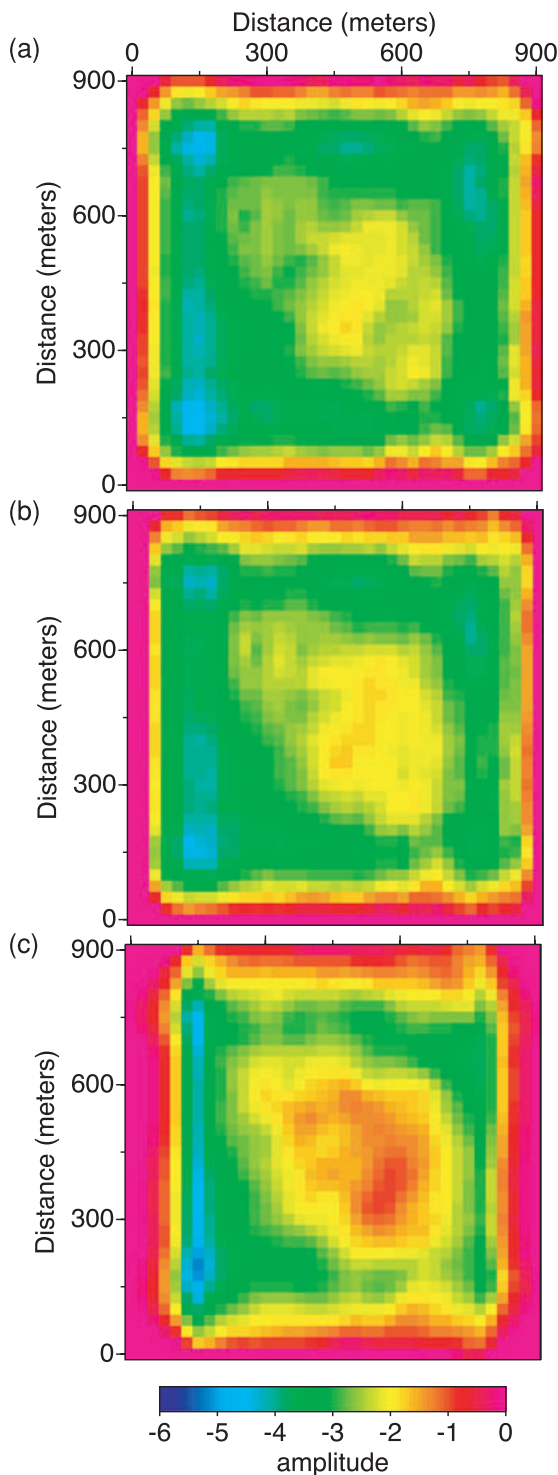


**Figure 11.** Seismic amplitudes for  $P$ -waves reflected from the fractured reservoir at angles of incidence of  $0^\circ$ ,  $20^\circ$  and  $36^\circ$ . All images are plotted with the same colour scale to facilitate comparisons.

simulations, corresponding to angles of incidence of  $0^\circ$ ,  $20^\circ$  and  $36^\circ$ . A simple phase shift migration was then applied to each common-offset synthetic result. Fig. 11 shows the reflection amplitude for each angle of incidence, and the increase of amplitude with angle is clear (note there are some artefacts along the boundaries because of the finite extent of the model). In regions where fractures are absent, toward the lower left corner of each figure, the reflection

amplitude is the most negative. In contrast, the fractures cause the reflection amplitude to change sign at the largest angle of incidence. This effect occurs because of the change in sign of the perturbation in the moduli  $C_{11}$  and  $C_{22}$ , which have greater influence at angles closer to horizontal. At larger angles of incidence, there is also less horizontal resolution in the image, which is why some features appear larger in that case.

## 5 CONCLUSIONS

This paper describes a method of modelling fracture distributions that relies on spatial correlation functions based on the elastic energy in the fractured medium, a rigorous physical basis for estimating distributions. While this method has been explored previously (Masihi & King 2007), we have extended the earlier work by presenting explicit tests of PBC implementations that help to reduce computation time and by exploring the use of constraints on fracture properties to match a priori values of orientation or length. Typical results show that when subsurface reservoir formation is isotropic and homogeneous, then this method generates orthogonal sets of fractures, a pattern that is commonly observed during basin formation or subsidence. While the absolute orientation of the fractures is non-unique, the final system can be rotated to match orientations desired in field-scale models, and we also presented results for constraining fracture lengths to match desired ranges of values. We also show how the fracture models generated using the SA algorithm can be used for seismic modelling by converting fracture models into crack density models. Effective medium theories can then relate crack density to reductions in seismic velocities caused by fracturing. Examples of synthetic seismograms computed using a ray-Born method suitable for the orthorhombic fracture models show amplitude variations that indicate variations in fracture density.

While the results presented in this paper are developed for a hypothetical field-scale model, it is important to note that it is straightforward to apply the same methods to field settings. While we chose arbitrary values to constrain fracture lengths and orientations, conventional field studies provide data that could be used to model a specific fractured formation. For example, orientations can be constrained by cores, image logs or seismic measurements, and outcrop, seismic or production data provide limits on fracture lengths. Therefore, the method is not restricted to simulations and will be suitable for field settings as well.

## ACKNOWLEDGMENTS

We acknowledge support from Dept. of Basic Energy Sciences (Award No. DE-FG03-00ER15034), and thank Kes Heffer and Mohsen Masihi for their helpful suggestions. We also thank Erik Saenger and an anonymous reviewer for helpful suggestions.

## REFERENCES

- Agersborg, R., Jakobsen, M., Ruud, B. & Johansen, T., 2007. Effects of pore fluid pressure on the seismic response of a fractured carbonate reservoir, *Stud. Geophys. Geod.*, **51**(1), 89–118.
- Angerer, E., Lanfranchi, P.H. & Rogers, S.F., 2003. Fractured reservoir modeling from seismic to simulator: a reality? *Leading Edge*, **22**, 684–689.
- Bakulin, A., Grechka, V. & Tsvankin, I., 2002. Seismic inversion for the parameters of two orthogonal fracture sets in a vti background medium, *Geophysics*, **67**, 292–299.
- Belayneh, M., Matthai, S.K. & Cosgrove, J.W., 2007. The implications of fracture swarms in the chalk of SE England on the tectonic history of basin

- and their impact on fluid flow in high-porosity, low permeability rocks, *Geol. Soc., Lond., Spec. Publ.*, **272**, 499–517.
- Beretta, M., Bernasconi, G. & Drufuca, G., 2002. AVO and AVA inversion for fractured reservoir characterization, *Geophys. Prospect.*, **67**, 300–306.
- Berkowitz, B., Bour, O. & Odling, N., 2000. Scaling of fracture connectivity in geological formations, *Geophys. Res. Lett.*, **27**(14), 2061–2064.
- Beydoun, W. & Mendes, M., 1989. Elastic ray-born  $l_2$ -migration/ inversion, *Geophys. J. Int.*, **97**, 151–160.
- Bour, O. & Davy, P., 1999. Clustering and size distributions of fault pattern; theory and measurements, *Geophys. Res. Lett.*, **26**(13), 2001–2004.
- Chapman, M., 2003. Frequency-dependent anisotropy due to meso-scale fractures in the presence of equant porosity, *Geophys. Prospect.*, **51**(5), 369–379.
- Coates, R. & Schoenberg, M., 1995. Finite-difference modelling of faults and fractures, *Geophysics*, **60**, 1514–1526.
- Daly, C., 2001. Stochastic vector and tensor fields applied to strain modeling, *Pet. Geosci.*, **7**, S97–S104.
- Darcel, C., Bour, O., Davy, P. & de Dreuzy, R., 2003. Connectivity properties of two-dimensional fracture networks with stochastic fracture correlation, *Water Resour. Res.*, **39**(10), 1272–1285.
- Gibson, R.L., Jr. & Thore, P., 2009. Seismic models of reflections from attenuating layers, *CSEG Recorder*, **34**(3), 44–49.
- Gibson, R.L., Toksoz, M.N. & Batini, F., 1993. Ray-born modeling of fracture-zone reflections in the larderello geothermal field, *Geophys. J. Int.*, **114**, 81–90.
- Grechka, V., 2005. Penny-shaped fractures revisited, *Stud. Geophys. Geod.*, **49**, 365–381.
- Grechka, V. & Kachanov, M., 2006a. Effective elasticity of rocks with closely spaced and intersecting cracks, *Geophysics*, **71**(3), D85–D91.
- Grechka, V. & Kachanov, M., 2006b. Seismic characterization of multiple fracture sets: does orthotropy suffice? *Geophysics*, **71**(3), D93–D105.
- Guéguen, Y. & Sarout, J., 2009. Crack-induced anisotropy in crustal rocks: predicted dry and fluid-saturated thomsen's parameters, *Phys. Earth planet. Inter.*, **172**(1–2), 116–124. [Diffusion, deformation and mineral properties of the Earth's interior. A Special Volume to honour the scientific contribution of Professor Olivier Jaoul]
- Hall, S.A., Kendall, J.-M., Maddock, J. & Fisher, Q., 2008. Crack density tensor inversion for analysis of changes in rock frame architecture, *Geophys. J. Int.*, **173**(2), 577–592.
- Heffer, K.J. & King, P.R., 2006. Spatial scaling of effective modulus and correlation of deformation near the critical point of fracturing, *Pure appl. Geophys.*, **163**(10), 2223–2242.
- Hudson, J., 1981. Wave speeds and attenuation of elastic waves in material containing cracks, *Geophys. J. R. astr. Soc.*, **64**, 133–150.
- Kachanov, M., 1980. Continuum model of medium with cracks, *J. Eng. Mech. Div., ASCE*, **106**, 1039–1051.
- Kachanov, M., 1992. Effective properties of cracked solids: critical review of some basic concepts, *Appl. Mech. Rev.*, **45**, 304–335.
- Kachanov, M., 1993. Elastic solids with many cracks and related problems, in *Advances in Applied Mechanics*, Vol. 30, pp. 259–445, eds Hutchinson, J. & Wu, T., Academic Press, San Diego, CA.
- Kachanov, M., Tsukrov, I. & Shafiro, B., 1994. Effective moduli of solids with cavities of various shapes, *Appl. Mech. Rev.*, **47**(1), S151–S174.
- Landau, L.D. & Lifshitz, E.M., 1982b. *Theory of Elasticity*, Butterworth-Heinemann, Pergamon, London.
- Liu, E., Hudson, J. & Pointer, T., 2000. Equivalent medium representation of fractured rock, *J. geophys. Res.*, **105**, 2981–3000.
- Masihi, M. & King, P.R., 2007. A correlated fracture networks: modeling and percolation properties, *Water Resour. Res.*, **43**, W07439, doi:10.1029/2006WR005331.
- Masihi, M., King, P.R. & Nurfaza, P.R., 2007. Fast estimation of performance parameters in fractured reservoirs using percolation theory, *SPE 94186-PA*, **12**(2), 167–178.
- Maultzsch, S., Chapman, M., Liu, E. & Li, X.Y., 2003. Modelling frequency-dependent seismic anisotropy in fluid-saturated rock with aligned fractures: implication of fracture size estimation from anisotropic measurements, *Geophys. Prospect.*, **51**(5), 381–392.
- Pointer, T., Liu, E. & Hudson, J.A., 2000. Seismic wave propagation in cracked porous media, *Geophys. J. Int.*, **142**, 199–231.
- Saenger, E.H. & Shapiro, S.A., 2002. Effective velocities in fractured media: a numerical study using the rotated staggered finite-difference grid., *Geophys. Prospect.*, **50**(2), 183–194.
- Sayers, C.M., 2002. Stress-dependent elastic anisotropy of sandstones, *Geophys. Prospect.*, **50**(1), 85–95.
- Sayers, C.M. & Kachanov, M., 1991. A simple technique for finding effective elastic constants of cracked solids for arbitrary crack orientation statistics, *Int. J. Solids Struct.*, **27**(6), 671–680.
- Sayers, C.M. & Kachanov, M., 1995. Microcrack-induced elastic wave anisotropy of brittle rocks, *J. geophys. Res.*, **100**, 4149–4156.
- Schubnel, A. & Guéguen, Y., 2003. Dispersion and anisotropy of elastic waves in cracked rocks, *J. geophys. Res.*, **108**, 2101, doi:10.1029/2002JB001824.
- Shekhar, R., 2008. Numerical Modeling of time-lapse seismic data from fractured reservoirs including fluid flow and geochemical processes, *PhD thesis*, Texas A&M University, College Station, Texas.
- Tod, S.R., 2001. The effects on seismic waves of interconnected nearly aligned cracks, *Geophys. J. Int.*, **146**(1), 249–263.
- Tran, N.H., 2007. Simulated annealing technique in discrete fracture network inversion: optimizing the optimization, *Comput. Geosci.*, **11**, 249–260.
- Vlastos, S., Liu, E., Main, I. & Li, X.Y., 2003. Numerical simulation of wave propagation in media with discrete distribution of fractures: effects of fracture sizes and spatial distributions, *Geophys. J. Int.*, **152**, 649–668.
- Vlastos, S., Liu, E., Main, I., Schoenberg, M., Narteau, C., Li, X.Y. & Mailhot, B., 2006. Dual simulations of fluid flow and seismic wave propagation in a fractured network: effects of pore pressure on seismic signature, *Geophys. J. Int.*, **166**, 825–838.
- Vlastos, S., Liu, E., Main, I. & Clement, N., 2007. Numerical simulation of wave propagation in 2-D fractured media: scattering attenuation at different stages of the growth of a fracture population, *Geophys. J. Int.*, **171**, 865–880.